CHAPTER 5

SUCCESSION AND BIOMASS ON WINTER SATELLITE IMAGERY

5.1 Background

Boreal forest is subject to disturbances such as fire or cut. On the permafrost, such disturbances can induce irreversible vegetation changes (Section 2.1). To manage a wide area of such boreal forests appropriately, it is required to apply forest inventory and monitoring methods by means of remote sensing that are reliable and robust for the specific local vegetation and climate (Section 1.5). In regard to this purpose, Chapter 4 described the unique growth pattern of larch stands in Central Yakutia. Following this, remote sensing techniques, empirical yet reflecting the local vegetation and climate, are to be discussed in this Chapter.

It was found in Chapter 4 that the larch stands became relatively sparser as the trees grew in terms of the relative spacing index. Sparse forest is not favorable for the conventional remote sensing observation because the forest floor can be seen from sensors and they are difficult to separate from the forest crowns. For example, GEMMELL (1995) found that the accuracy of the timber volume estimation was reduced at where the volume was lower than 150 m^3/ha because of the forest floor at the low-stocked stands. Especially in Central Yakutia, where surface fires often occur, the burned scars change the reflectance much, even if the standing trees are still alive. In Chapter 3, it was also found that the indices from summer image were unstable or very quickly recovered through time after disturbances. Instead, indices from winter images with snow were favorable because the snow hided anything on the ground and made the forest floor a monotonous medium (Section 2.2).

Simple composition of snow, trees and their shadow in forest stands is suitable for applying the geometric-optical models, which predict the proportion of forest floor, tree crowns, and their shadow from the three dimensional shape of tree crowns and the allocation of the sun and the sensor (Section 1.3). It is a common characteristics throughout such models that in a multi-spectral space a trajectory from the pure floor to the completely closed canopy draws not a straight line but a curve swinging by the

dark shadow. The real stands can be found along such trajectory in the multi-spectral space, and inversely the stand condition can be explained from the location on the space.

The objectives of this Chapter are;

- To observe the distribution of forest stands on a multi-spectral space.
- To create some empirical stand estimation models from the winter image.

5.2 Study Area

The study area is identical to that of Chapter 4. See Section 4.2.

5.3 Methods

5.3.1 Ground Truths

Out of the 26 measured stands in Chapter 4, 23 stands are used for the further analyses. Other three stands, namely, M3, M11, and M21, are dropped because the locations are apparently on slope. See Table 4.1 for stand parameters and the satellite image digital number (DN) as described below.

5.3.2 Image Used and the Preprocessing

The satellite image used in this study is a Landsat ETM+ image acquired on 30 October 1999 (Path/Row = 122/016) (Figure 5.1). The sun elevation angle is 13°. At the moment of image acquisition, the entire water surface but a small part of Lena River frozen, and almost all the open ground surface and the frozen water were covered by snow. A summer ETM+ image on 28 Aug. 1999 (Path/Row = 122/017) is combined with the winter image for the classification and the comparison (Figure 5.2).

The image is clipped in an area of 75km by 60km and georeferenced to the topological maps of the scale of 1:200,000. Dark object retrieval (CHAVEZ *et al.*, 1994) is applied to remove the atmospheric effect in dark portion of the image. There are thin clouds overcastting shadows on the ground. To adjust the income radiation from the sun, local snow reflections from open lands are used with an assumption that the snow reflectance at that time is constant over the study area. For each reflective band of the

image, the DNs of snow-cover on open lands are interpolated over the image, then the DNs of whole pixels are stretched using the ratio of local snow-cover reflection to the highest snow-cover. The forests on the image are stratified using unsupervised classification so that the ground survey plots are efficiently selected.

Only two spectral bands of a sensor are required to decompose a pixel into the three endmembers of floor, tree canopy and its shadow. The farer an endmember locates from the others on the two-dimensional space, the more accurately a pixel can be decomposed. When foliated vegetation is to be observed with this technique, a visible band and a near-infrared band are usually used because the soil (or snow) is bright at both bands while the vegetation is bright at the near infrared and dark at the visible (*e.g.* NAKAZONO *et al.*, 2000; ONO and FUJIWARA, 2002; FERNANDES *et al.*, 2002). However, if the vegetation is deciduous, it is not the case during the defoliated season.

Among six reflection bands of the Landsat ETM+ image, visible band 2 (B2) and mid-infrared band 5 (B5) are used for the analyses, because non-foliage organ has rather even reflectance through the wavelengths (GOWARD *et al.*, 1994) while snow has a very high visible reflectance and a low mid-infrared (MIR) reflectance (DOZIER, 1989, see Figure 2.3). Mean digital numbers (DN) of 3 x 3 pixels around the plot location for the two bands are assigned as the image values of each measured plot.

5.3.3 Scattergram and Empirical Models

Scattergrams of the measured stands on the B2-B5 space are drawn with stand parameters, that is, mean DBH, basal area, and the stand IDs. If a reflectance model that explains the stand reflectance were available, it would have been possible to fit the model to the measured stands on the scattergram. Unfortunately, however, such model for defoliated larch stand has not been developed yet. In the present study, thus, the scattergrams will be interpreted and intuitively regression models are to be applied.

Results from empirical regressions on a single image would not be able to apply directly and universally to other images, but interpretation based on the

geometric-optical reflectance model would make some insights for further development.

5.4 Results and Discussion

5.4.1 The Scattergram

The scattergram of the visible and MIR bands are shown in Figure 5.2 with the stand ID, the mean DBH, the basal area of each stand on it. It is apparent that the cloud of stands makes a 'V' shape from an almost open stand at the upper right to a very dense stand at the upper left through intermediate stands at the lower left. It should be noted, however, that the succession does not follow the V curve; at the most crowded part of the upper left relatively small tree's stands gathered and the biggest stands located at the darkest part of the lower left. JAKUBAUSKAS (1996) confirmed a similar result for pine stands in a dry area. He assumed that in the early stage of succession an open stand moves to the densest stand directly rather than along the 'V' curve. This is also supported by the results of Chapter 4, where the young stands with high number of trees are relatively denser in terms of the relative spacing index while the more matured stands with big trees are relatively sparser.

This phenomenon can be described as follows; a cleared stand has no or a few standing trees that cast shadows on the floor, which is why it is as nearly bright as snow (at the upper right of the scattergram). As trees regenerate, canopy immediately closes, which results in an even reflectance close to a reflectance of pure non-foliage organ (at the upper left). Though the transparency of the defoliated canopy is higher than in summer, the chance of seeing shadow on the floor is low because the canopy is dense and homogeneous. As trees grow, the canopy becomes uneven that makes the chance of seeing shadow on the floor higher (COHEN *et al.*, 1995; JAKUBAUSKAS, 1996). In addition, the stand becomes relatively sparser that makes more chance of seeing shadow on the floor. As the chance of seeing shadow increases, the reflectance becomes darker (to the lower left). The very high reflectance of snow in the visible band makes the dense even canopy distinguishable from the cleared stands (Figure 5.3).

5.4.2 Empirical Models for Estimating the Stand Parameters

From the interpretation of the scattergram, some empirical relationships between the image and the stand parameters are derived. As basal area grows, the visible reflectance becomes lower, because more trees cast more shadow on the floor resulting less sunlit snow observed from above. This is supported by an analysis of hemispherical photos (TAKAO, in press). Here, assuming the visible reflectance attenuates with the basal area, G, the pixel value of B2, DN_{B2}, is correlated as equation (5.1) (Figure 5.4(a)).

$$DN_{B2} = 88.1 - 23.2 \log G, \qquad R^2 = .74,\ n = 23 \tag{5.1}$$

The basal area becomes saturated at around 25 [m²/ha] (Chapter 5), which means the DN_{B2} would be saturated at around 56 by equation (5.1). The stands with DN_{B2} of around this value should be in the normal condition (Chapter 4). In addition, as in the previous section, the succession appears vertically from upper left to lower left on the scattergram (Figure 5.2). Here, the stands with DN_{B2} less than an intuitively set threshold 65 are assumed as normal, and the pixel value of B5, DN_{B5}, is correlated to mean DBH, as an indicator of succession, as equation (5.2) (Figure 5.4(b)).

$$DN_{B5} = 25.7 - 7.6 \log DBH, R^2 = .51,\ n = 17 \tag{5.2}$$

The above-ground biomass (AGB) was well explained by the combination of the normality (basal area) and the succession stage (mean height or stand density) (equations 4.16 and 4.17). Here, mimicking these structures and the AGB is fit by both the bands as equation (5.3) (Figure 5.4(c)).

$$\log AGB = 3.92 - .028\, DN_{B2} - .034\, DN_{B5}, \qquad R^2 = .69,\ n = 23 \tag{5.3}$$

Finally, leaf area index (LAI) is fit as equation (5.4) (Figure 5.4(d)). Though larches are defoliated in winter, the mass of leaf can be estimated by allometric relation (equation 4.8) and the mass can be converted to the LAI by the mass per leaf area, or

137.9 g/m^2 (VYGODSKAYA *et al.*, 1997). For comparison, NDVI (normalized differenced vegetation index) derived from the summer image is also fit to LAI as equation (5.5) (Figure 5.4(e)).

$$DN_{B2} = 60.0 - 20.56 \log LAI, \qquad R^2 = .69,\ n = 23 \qquad (5.4)$$

$$NDVI = .502 - .124 \log LAI, \qquad R^2 = .58,\ n = 23 \qquad (5.5)$$

Here, the winter image got a better fit on LAI than the summer image did. This might be because of the effect of the floor vegetation on the summer image. This is an evidence of the advantage of winter image for the forest observation.

Using the derived relationships (inverse of equation 5.2, and equation 5.3), the distribution of the mean stand DBH and the AGB are estimated using the image (Figure 5.6 (a) and (b), respectively). From these figures, one can interpret that mainly young and less stocked forest distribute on the east bank of Lena River, where the forest is not strictly protected as the opposite side around the City of Yakutsk. On the west bank, in general, the forests are well stocked, but some stands are apparently on the young stage supposedly after fires.

There are some issues becoming apparent during the analyses. The low sun elevation angle makes severe uneven brightness on slopes. Though the major part of the study area is very flat, it might be possible that gentle slopes are also affected in some degree. In addition, because of the low angle, the shadow reaches as far away as cot 13° = 4.3 times of the tree height, *e.g.* for a tree of 20m height the shadow is cast about 90m away from its base. This would lead to unreliable results on the forest edges and at patchy aggregations of small stands.

In the DBH fitting (equation 5.2), there seems to be a tendency that the mixed stands with birches have dark DN_{B5} for their DBH. Among the measured stands, pure larch stands are M1, M2, M5, M6, M14, M15, M20, M23, and M24, while stands which contain other species' basal area more than 1/3 of the total are M7, M10, M16, M19, M25, and M26. Major part of the other species is birch, which has thinner branches for DBH comparing to the larch. If birches occupy in the canopy as do in the basal area, it

can be supposed that holes with few branches appear amid the larch crowns with many branches during defoliated season. These holes allow the forest floor, which is well shaded, to be seen well from above, that would be the reason why such mixed stands become darker in MIR, resulting in the DBH overestimation. Methods to separate birches from larches will be required.

5.5 Summary of Chapter

Following the analyses of the larch stand growth in Chapter 4, the relationships between these stand parameters and a winter satellite image were analyzed in light of the geometric-optical relationship among the forest floor, tree crowns, and their shadow. The bands used were a visible band 2 and a mid-infrared band 5, which best separate the reflectance of snow, canopy and shadow. The empirical regressions enable to inversely estimate from the satellite image the basal area, DBH, AGB, and LAI, even though the trees were defoliated in this season. Though these specific analyses on an image would not be able to apply universally, the results and insights would contribute to further developing generalized geometric-optical models of the defoliated trees on snow.

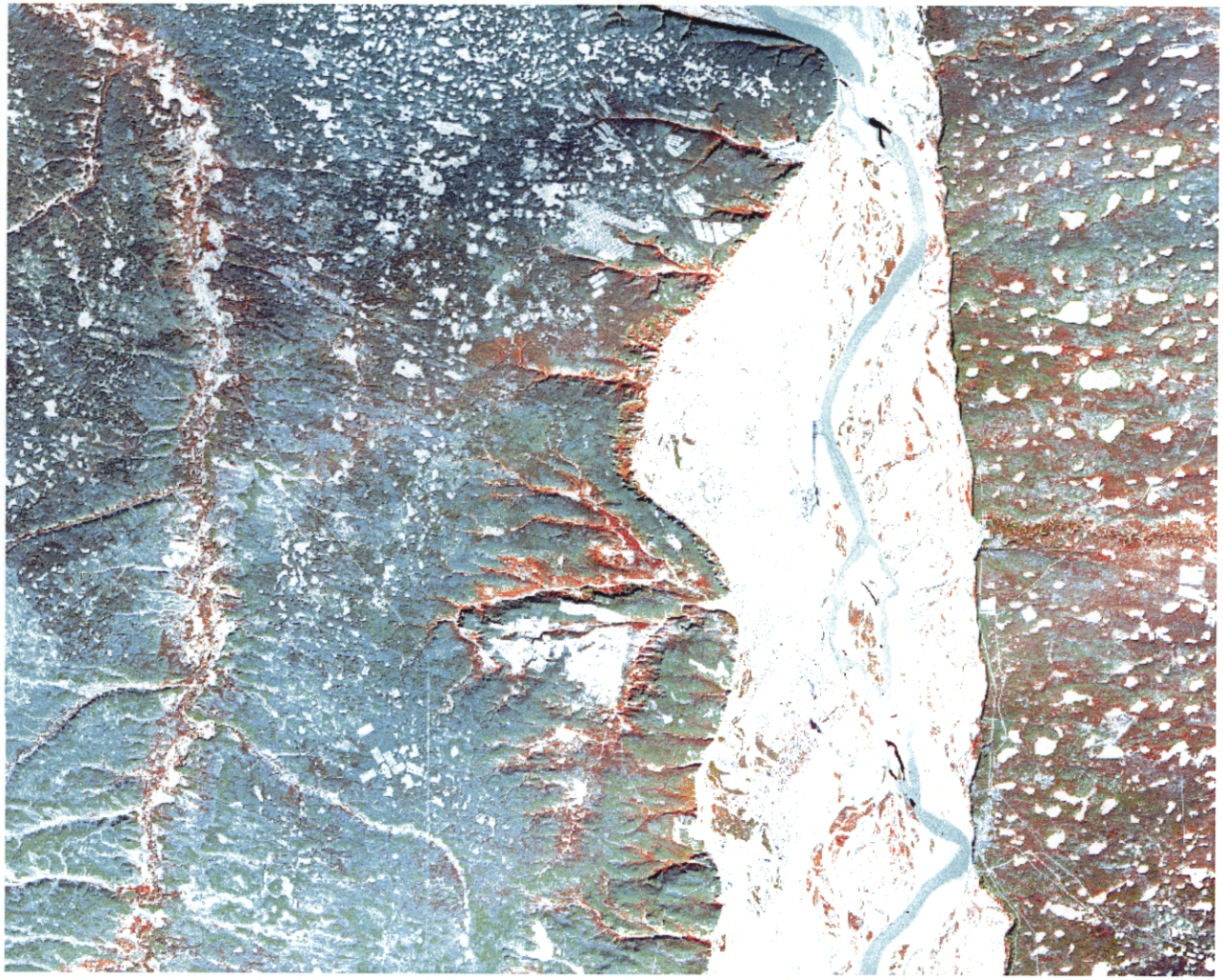

Figure 5.1 Winter image used for the analyses

LANDSAT ETM+ 1999-10-30, path/row = 122/016, RGB = Band 5,4,2

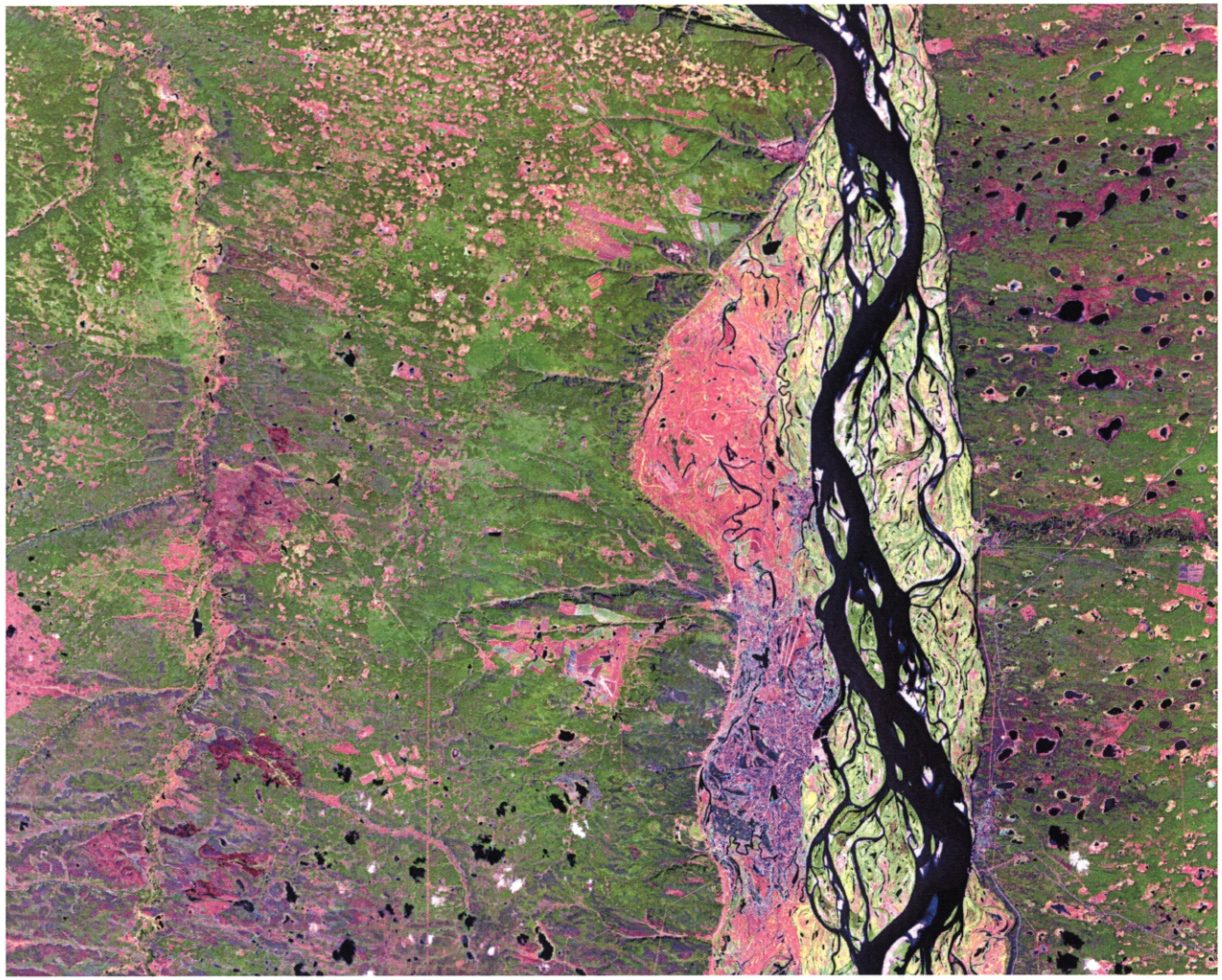

Figure 5.2 Summer image used for the analyses

LANDSAT ETM+ 1999-08-27, path/row = 122/017, RGB = Band 5,4,3

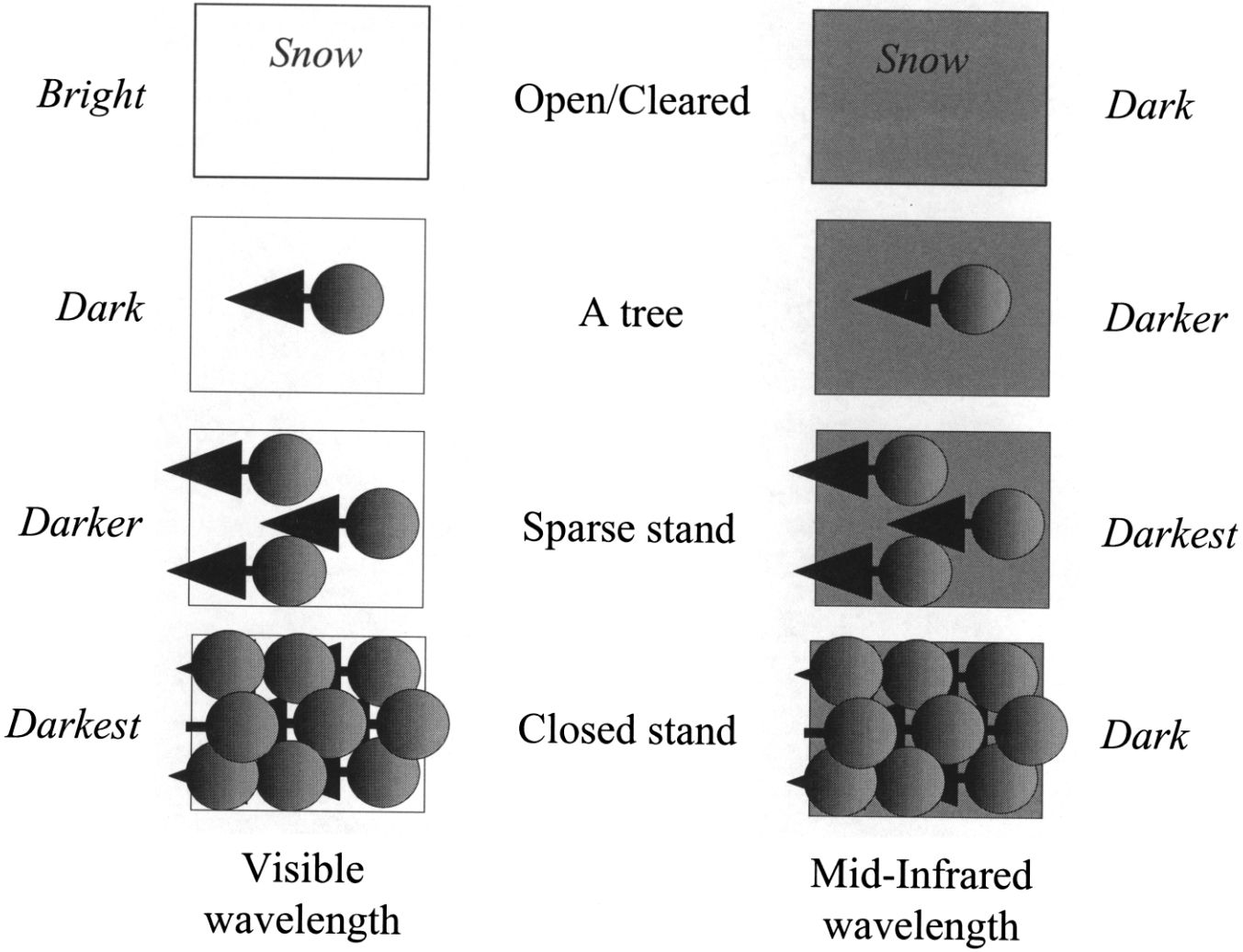

Figure 5.3 Conceptual diagram of the reflectance of boreal forest during winter

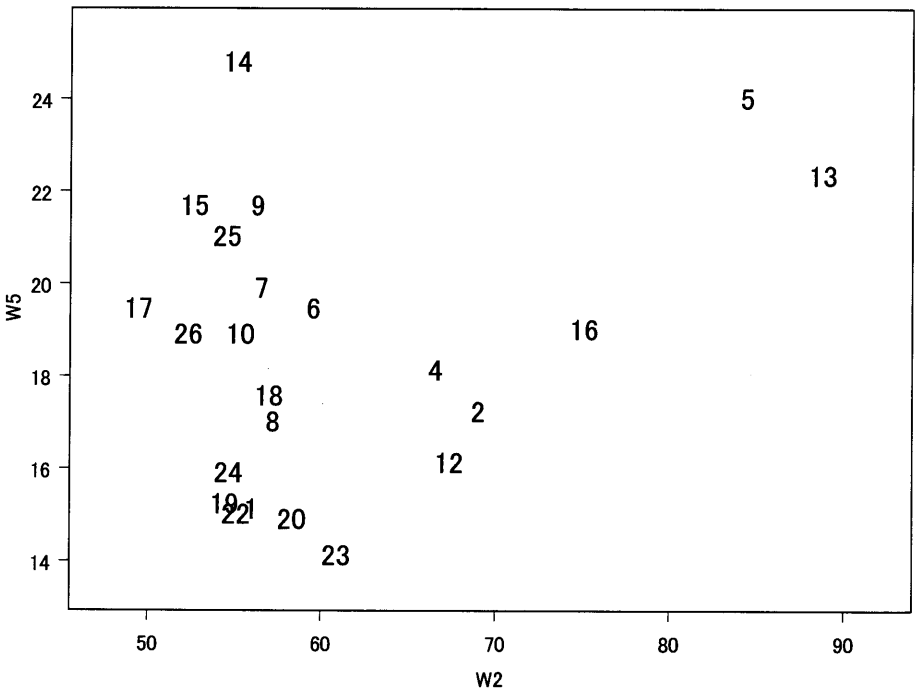

(a) Stand ID

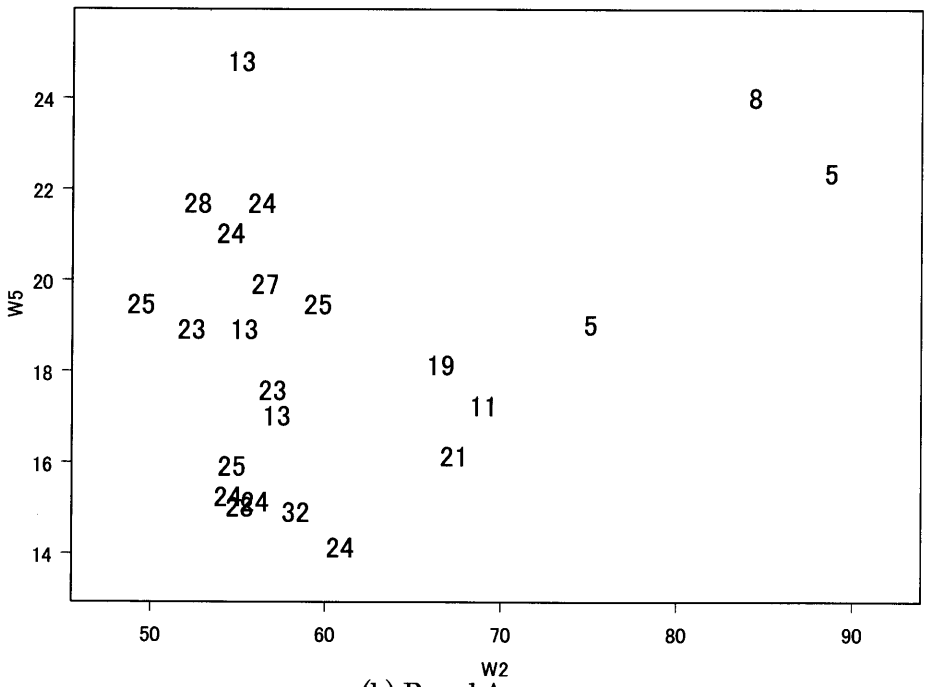

(b) Basal Area

Figure 5.4 Larch stands distribution on the visible – mid-infrared space
W2 and W5 denote Band 2 (visible) and Band 5 (MIR) of the winter ETM+ image.
The numbers in the graphs represent (a) Stand ID, (b) Basal area [m^2/ha], and (c) Quadratic mean DBH [cm], respectively.

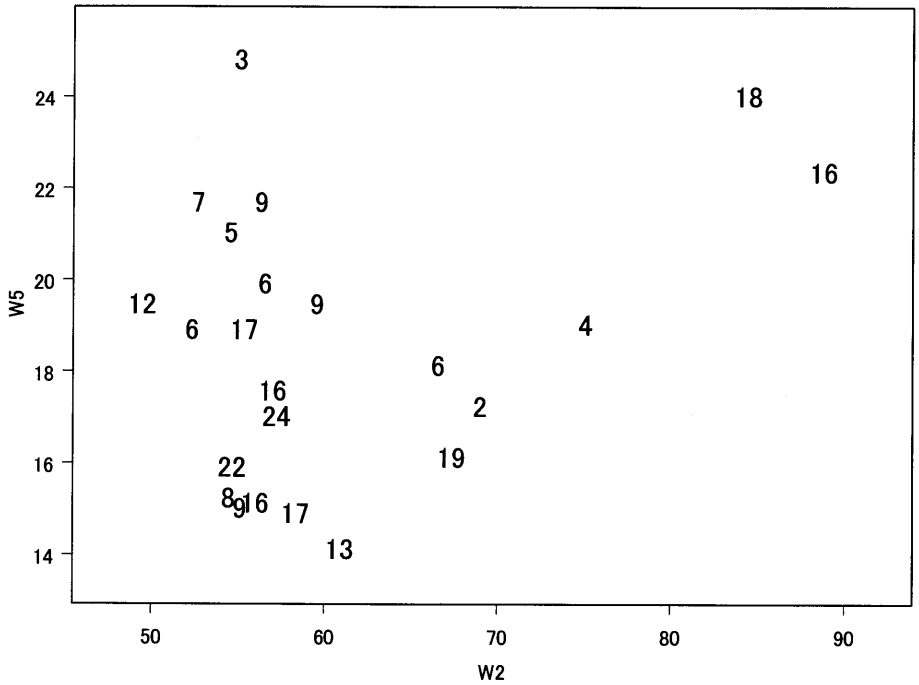

(c) Quadratic Mean DBH

Figure 5.4 (continued)

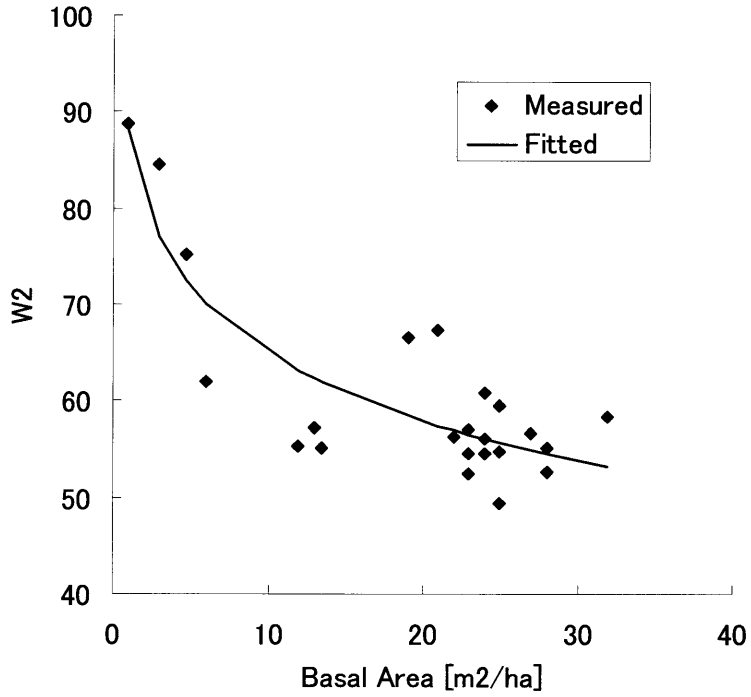

(a) Basal Area

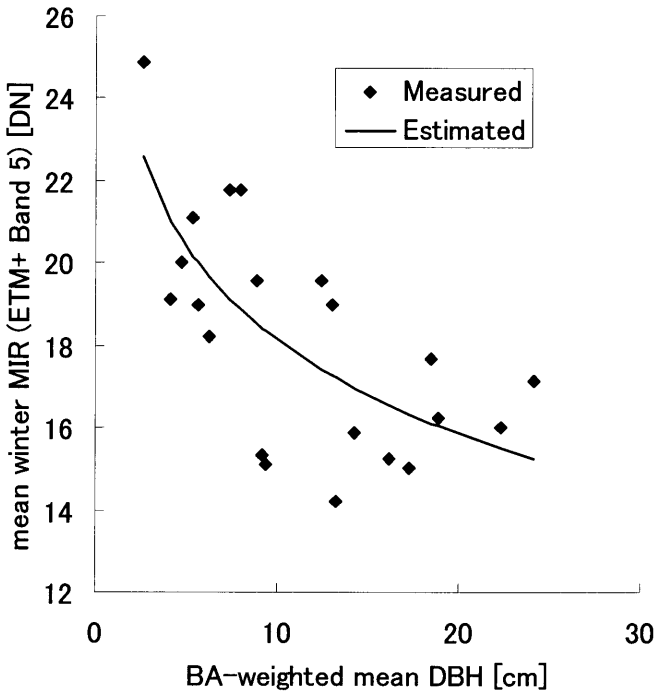

(b) Quadratic Mean DBH

Figure 5.5 Stand parameter relationships and estimations from satellite images

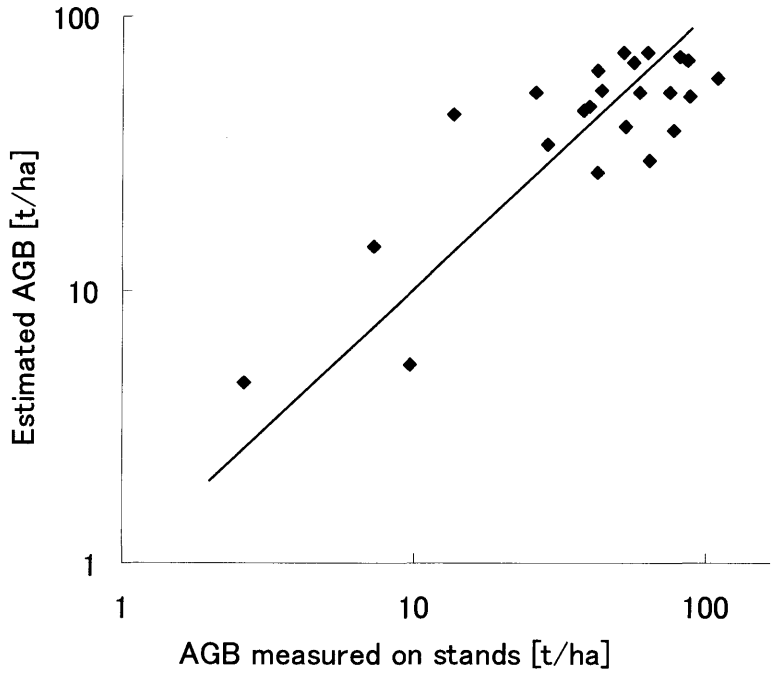

(c) Above-Ground Biomass

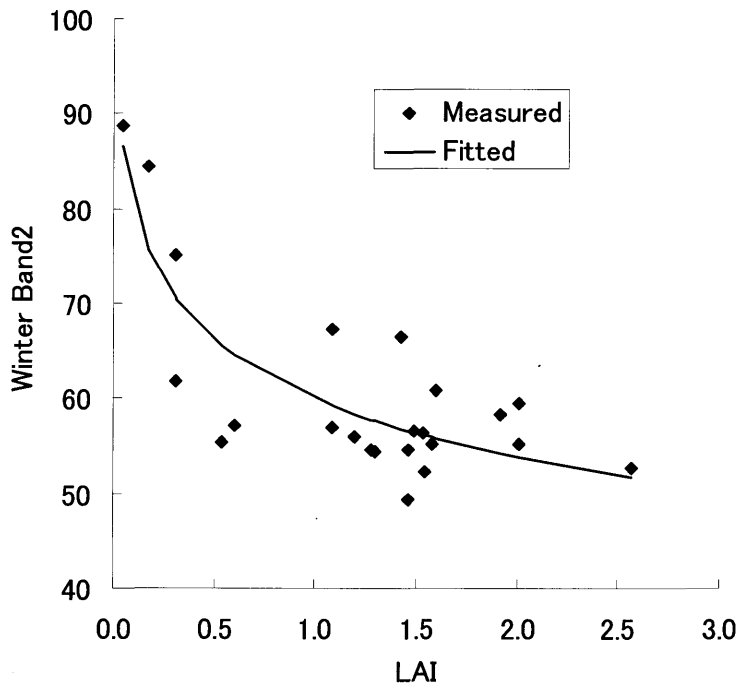

(d) Leaf Area Index by Winter Image

Figure 5.5 (continued)

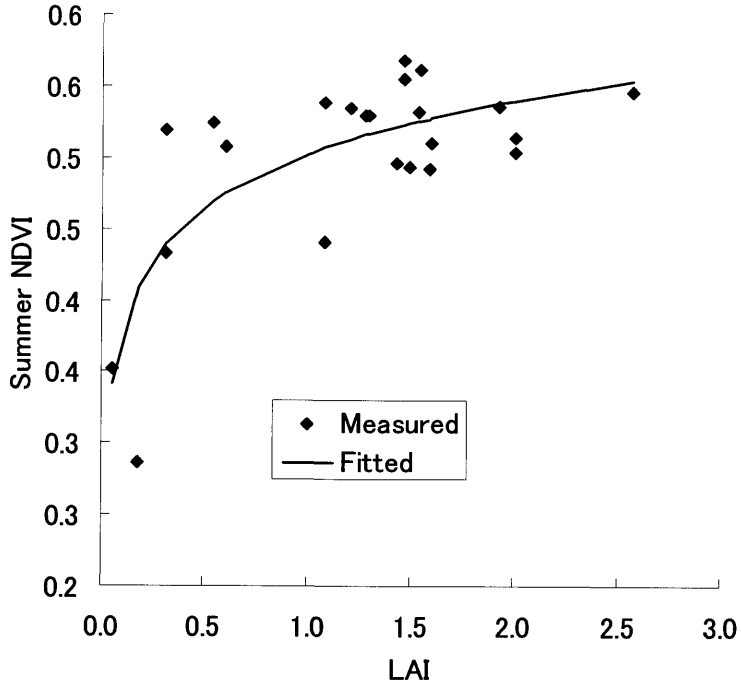

(e) Leaf Area Index by Summer Image

Figure 5.5 (continued)

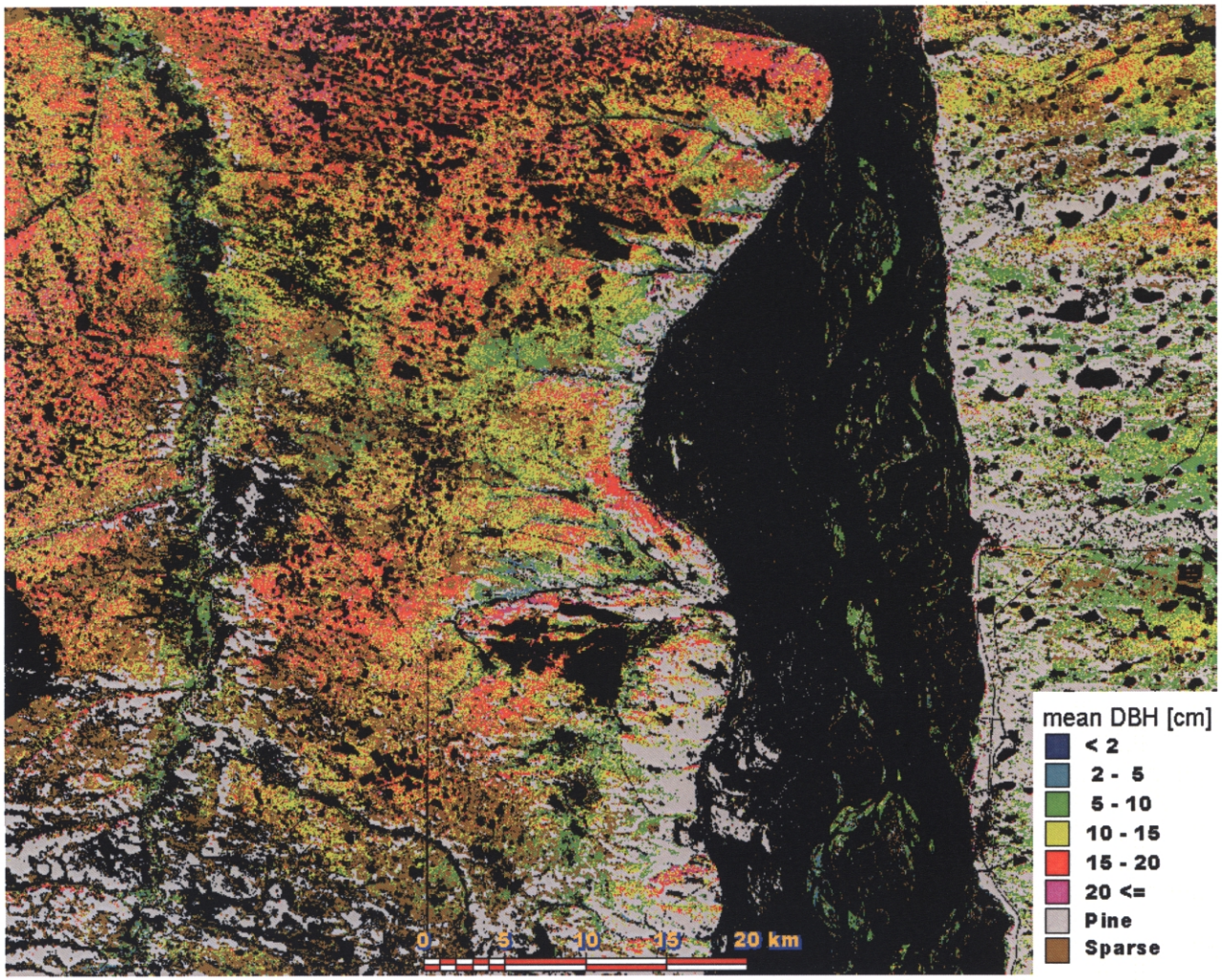

Figure 5.6 (a) Mean DBH Estimation by Winter Satellite Image

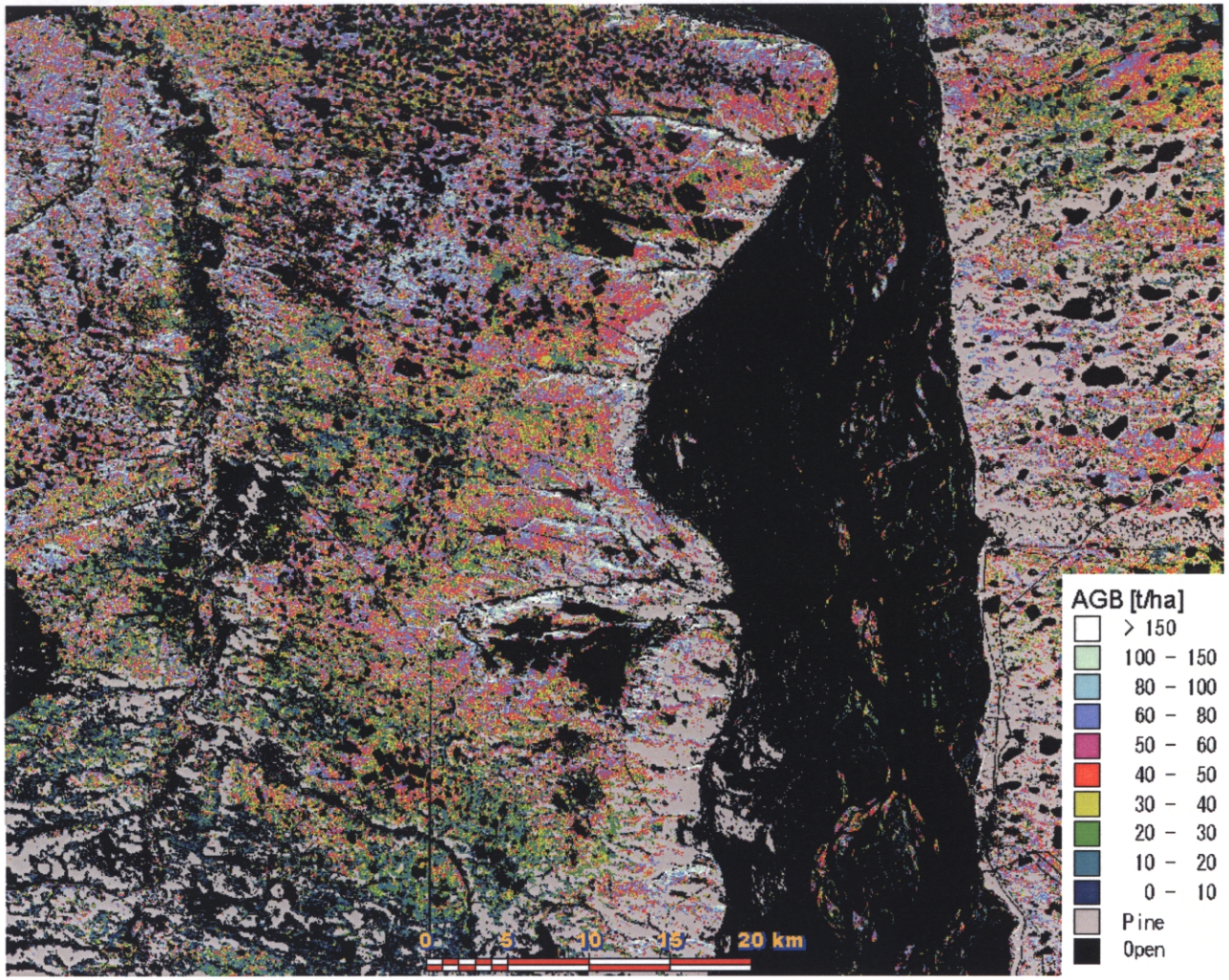

Figure 5.6 (b) Mean DBH Estimation by Winter Satellite Image